

Article

Multi-Port PWM DC-DC Power Converter for Renewable Energy Applications

Abdulaziz Almutairi ¹, Khairy Sayed ², Naif Albagami ^{1,*}, Ahmed G. Abo-Khalil ^{1,3} and Hedra Saleeb ⁴

¹ Electrical Engineering Department, University of Majmaah, Almajmaah 11952, Saudi Arabia; ad.almutiri@mu.edu.sa (A.A.); a.abokhalil@mu.edu.sa (A.G.A.-K.)

² Electrical Engineering Department, Faculty of Engineering, Sohag University, Sohag 82524, Egypt; khairy_sayed@eng.sohag.edu.eg

³ Electrical Engineering Department, Assiut University, Assiut 71515, Egypt

⁴ Electrical Department, Faculty of Technology and Education, Sohag University, Sohag 82524, Egypt; hedra_saleeeeb@yahoo.com

* Correspondence: n.albagami@mu.edu.sa

Abstract: In this paper, a new multi-port DC-DC power converter used to deal with the intermittent nature and slow response in renewable energy applications is proposed. The proposed converter integrates a DC-DC converter and a DC-AC inverter, and the proposed circuit integrates various renewable energy sources in addition to the energy storage unit. By combining renewable energy sources with a statistical trend to offset each other, the impact of the intermittency can be considerably minimized. This combination increases the overall system reliability and usability. Moreover, integrating such systems with energy storage systems can overcome the slow response issue of renewable sources. It can provide the additional energy required by the load or absorb the extra energy provided by the power sources, which greatly improves the dynamics of the overall system. The proposed converter can reduce the system cost and size and improve the efficiency and reliability. The operation principle is studied in detail, and the design considerations are provided. The proposed architecture and its control strategy were analyzed and studied using the Simulink/MATLAB environment. Finally, the feasibility of the proper operation of the studied converter was experimentally verified based on the results of experimental studies conducted on a 300 W prototype implemented in a laboratory.

Keywords: DC-DC converter; multi-port converter; Maximum Power Point Tracking (MPPT); renewable energy



Citation: Almutairi, A.; Sayed, K.; Albagami, N.; Abo-Khalil, A.G.; Saleeb, H. Multi-Port PWM DC-DC Power Converter for Renewable Energy Applications. *Energies* **2021**, *14*, 3490. <https://doi.org/10.3390/en14123490>

Academic Editor: Ricardo J. Bessa

Received: 5 May 2021

Accepted: 8 June 2021

Published: 12 June 2021

Publisher's Note: MDPI stays neutral with regard to jurisdictional claims in published maps and institutional affiliations.



Copyright: © 2021 by the authors. Licensee MDPI, Basel, Switzerland. This article is an open access article distributed under the terms and conditions of the Creative Commons Attribution (CC BY) license (<https://creativecommons.org/licenses/by/4.0/>).

1. Introduction

Solar energy, wind energy, and tidal and biomass energy, as the main forms of clean energy technologies, have become the true solution to the recent energy crisis worldwide. Natural energy sources, such as coal, oil, natural gas, and nuclear materials, are limited and cause pollution, and thus, to meet the dramatically increasing demand for energy, clean and renewable energy technologies, such as wind and photovoltaic (PV) energy, have been widely deployed over recent decades [1,2]. Renewable energy systems will herald the most substantial advances in energy efficiency, energy saving, and environmental protection over the next few decades [3]. Grid-connected renewable energy systems are usually a more suitable choice for locations near a power grid because energy storage systems are currently unsatisfactory. Wind and PV energies complement each other because sunny days are often calm and heavy winds usually arise at night or on overclouded days. The combination of the PV module and wind energy module will reduce the zero-power periods. Therefore, solar/fuel cell/wind hybrid generation systems have a higher obtainability to supply continuous electrical energy than any other single source. In recent years, there has been a large focus on developing renewable energy applications. While significant improvements

have been made in renewable energy applications, there are some essential limitations in these applications. Owing to these limitations, solar and wind energy systems are intermittent natural sources. Moreover, the dynamics of the electrochemical reaction of a fuel cell are quite slow compared to the electrical load. This is unacceptable for recent power systems that require a constant voltage and a constant frequency voltage source.

Distributed generation (DG) units are small-scale electrical power supplies connected together in a microgrid [2]. DG units based on renewable energy resources, such as solar, wind, and biomass, have been widely deployed owing to their numerous advantages. DG technologies can offer customers with energy needs that are environmentally friendly, more cost-effective, and provide higher energy reliability and power quality than traditional solutions. The DG provides electrical power at locations closer to customers than a central generation plant. Hence, implementing DG units in electric distribution systems is one of the key solutions for supplying electrical power to consumers. Another benefit of DG is that it can reduce the peak load demand and total charges of energy usage, as well as guarantee better power quality and reliability. The DG power rating ranges from a few kilowatts to 50 MW.

Hybrid distributed generation systems (HDGs) are a good solution for regions with traditional energy shortages aiming to adopt solar/fuel cell/wind energy in DG systems, which take advantage of both DG systems and renewable energy systems. To install such a hybrid renewable energy system, a two-input single-output scheme has been developed in several studies [4,5]. Multi-input DC-DC power converter topologies are used to accommodate the variations in hybrid renewable energy, allowing power to be transferred from different input voltage sources to the output. As described in [4], a single-input, dual-input converter was developed for a combined solar/wind energy generation system. Both the PV array and wind turbine were utilized. In [5], a high-frequency transformer (HFT) was utilized to achieve an electrical or galvanic isolation advantage. In addition, a full-bridge dual-input DC-DC power converter with variable pulse-width-modulated (PWM) control can be realized to provide a potential approach to integrating power from diverse sources into a high-frequency-link isolated circuit. However, these circuits cannot be connected to backup power banks (utility or batteries). Hence, they are unsuitable for DG PV panels/fuel cells/wind turbine hybrid generation systems.

In many applications, it is necessary to associate several renewable energy sources of dissimilar types (e.g., solar PV and wind) and integrate them into a microgrid [6–11]. Multi-port DC-DC power converters are proposed to apply efficient power management and grid integration for multiple sources. This work proposes a new power converter circuit that can overcome the problems of intermittent features and the slow response of renewable energy sources. The proposed converter topology integrates several renewable energy sources in addition to energy storage units. The effect of the intermittent nature can be greatly minimized by integrating renewable energy sources. These sources compensate for each other. However, this integration increases the reliability and obtainability of the entire system. Furthermore, integrating the energy storage overcomes the slow response problem of renewable sources. Thus, an energy storage unit can offer the additional energy required by the load or utilize the excess energy delivered by the renewable sources. This will significantly improve the dynamics of the overall system.

Figure 1 shows a multisource, grid-connected, two-stage, hybrid renewable energy system composed of a multi-port DC-DC power converter and a PWM DC-AC power inverter [12]. The DC-DC converter connects several sources, such as photovoltaic (PV) modules, fuel cells (FCs), and wind turbine generators (WTGs), to multiple input ports. The multi-port DC-DC power converter not only adjusts the DC output of the sources to a regulated DC voltage required for inverter input, it can also afford several essential control functions, such as tracking the maximum power point (MPPT), for different renewable sources. Some of the necessary design considerations and key advantages of the proposed system are as follows:

Lightweight and compact size.

- # Enhanced efficiency and high reliability.
- # Effective utilization of wind and solar PV energy.
- # The capability of integrating various sources.
- # Delivery of an alternative power source for loads when the power delivered by local generators cannot fulfill the microgrid load.

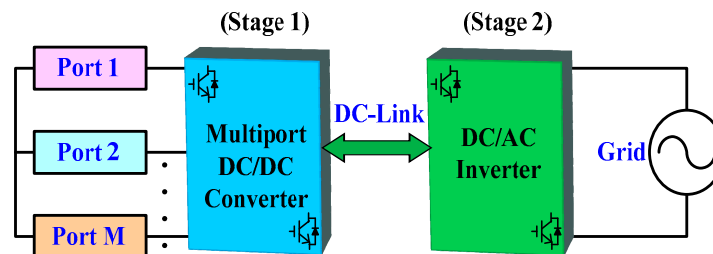


Figure 1. Block diagram of a two-stage, multi-port, and grid-connected power system configuration.

The remainder of this paper is organized as follows. Afterward, a survey of previous studies is introduced to the multiport DC-DC power converter described in Section 1. The proposed converter topology and operation principle are analyzed in Section 2. The control strategy for the proposed multiport DC-DC power converter is described in Section 3. In Section 4, a dynamic simulation model of the multiport DC-DC power converter is formulated and implemented in a MATLAB/Simulink environment (Version R2018b, Natick, Massachusetts, USA), using the design concerns for the studied converter. The experimental results are presented in Section 5 to verify the effectiveness of the treated multi-port DC-DC power converter for simultaneous MPPT control of hybrid PV panels/fuel cells/wind turbine systems. Section 6 summarizes this study with certain concluding observations.

The main contribution of the manuscript

- # A multi-port DC-DC power converter is proposed for the integration of three renewable energy sources (PV panels, fuel cells, and wind turbines) and an energy storage source (batteries or supercapacitors).
- # An energy management system was developed.
- # A simulation model was proposed for energy management strategy to achieve an efficient power utilization.
- # The battery energy storage compensates for the slow response of the fuel cells and photovoltaic units.
- # The proposed strategy can share power between DG units, even under a different renewable power generation.
- # An experimental prototype was applied to verify the effectiveness of the proposed multi-port converter topology.

2. Proposed Converter and Operation Principle

A new multi-port DC-DC power converter is proposed for the integrated power management of many renewable energy sources, and consists of PV panels, fuel cells, and a wind turbine hybrid generation system, in which only one switch is used for each input port connected to a source, as shown in Figure 2. This first converter cell comprises a boost inductor L_1 , an active switch S_1 , a diode D_1 , and a filtering capacitor C_{dc} at the output, as shown in Figure 2. Figure 2 presents the circuit diagram of the proposed multi-port DC-DC power converter, and the given parameters of the circuit are shown in Table 1. This converter circuit is composed of three ports in parallel, in addition to a battery bank, as an energy storage unit. Each port comprises a semiconductor power switch, power diode, and boost inductor. However, the proposed multiport DC-DC converter circuit has the fewest number of components, and hence, a proper cost as compared with the present multi-port DC-DC power converter circuits [13–20].

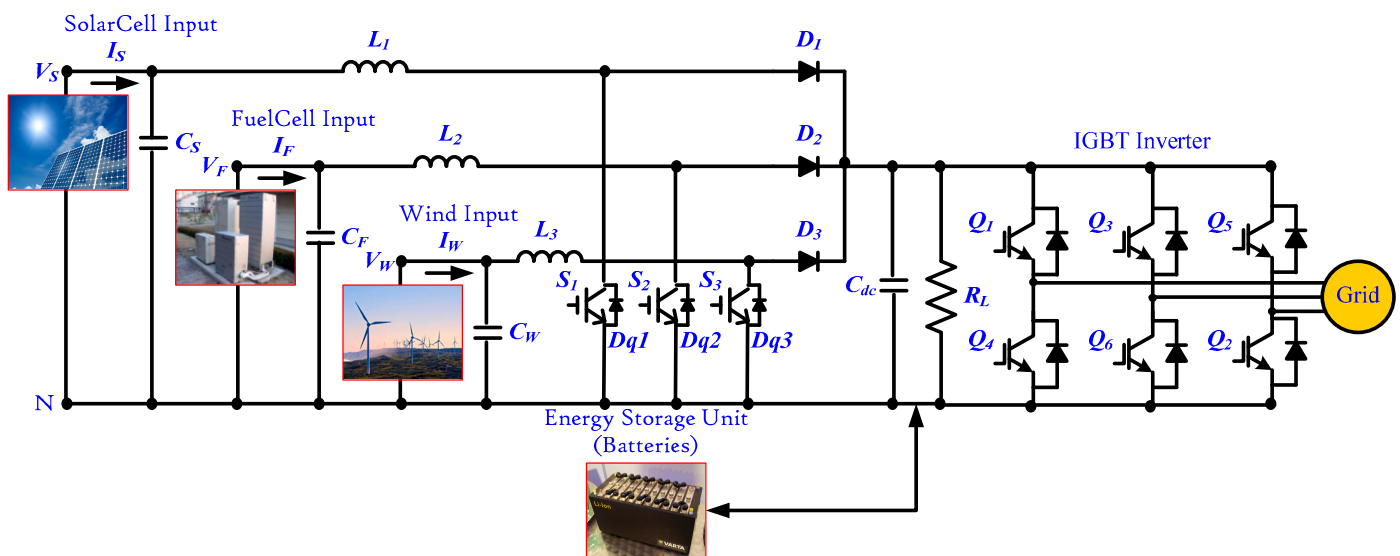


Figure 2. Block diagram of the proposed multi-port DC-AC power converter topology.

Table 1. Values of circuit parameters.

Item	Symbol	Value
Inductor turns number	T_{No}	25
Used core	Ferrite Core (UU-95)	
Self-Inductance of Inductor 1	L_1	420 μ H
Self-Inductance of Inductor 2	L_2	280 μ H
Self-Inductance of Inductor 3	L_3	300 μ H
Solar Port Filter Capacitor	C_S	100 μ F
Fuel Cell Port Filter Capacitor	C_F	330 μ F
Wind Port Filter Capacitor	C_W	100 μ F
Filtering Capacitor	C_{dc}	330 μ F

2.1. Driving Signal Scheme

Figure 3 schematically shows the gate-pulse control signals of the S_1 , S_2 , and S_3 main switches of the proposed converter (Figure 2). The implementation of an N-parallel-cell converter was studied. If the parallel cells are controlled using a synchronous clock, as displayed in Figure 3a for a three-parallel-cell system, this system achieves a performance close to that of a single high-power converter. However, if these cells are controlled individually and, hence, clocked at different switching frequencies, as illustrated in Figure 3b, the current ripples in the converter output and input will be considerably minimized owing to a passive ripple cancellation that arises among the cells.

The well-known interleaving clocking method is illustrated in Figure 3c. To interleave N parallel-connected (or series-connected) converter cells, active switches are switched at the same frequency as the switching operation, but pulses are phase-shifted by $2\pi/N$ radians [21]. The proposed converter can be boosted by turning on the active switch of any particular cell (S_1 , S_2 , or S_3) simultaneously.

In the interleaved clocking technique, all cells are switched on and off at the same frequency, while operation waveforms shift in phase during the switching cycle. The advantages of this technique include a harmonic reduction among the cells and a higher ripple frequency and lower ripple amplitude in the input and output waveforms, which are easy to filter [21]. For a wide class of converter topologies, the N-cell interleaving clocking yields an N-fold increase in the ripple current fundamental frequency and a magnitude decrease in the peak ripples by a factor of N or more when compared with synchronized clocking [22–25].

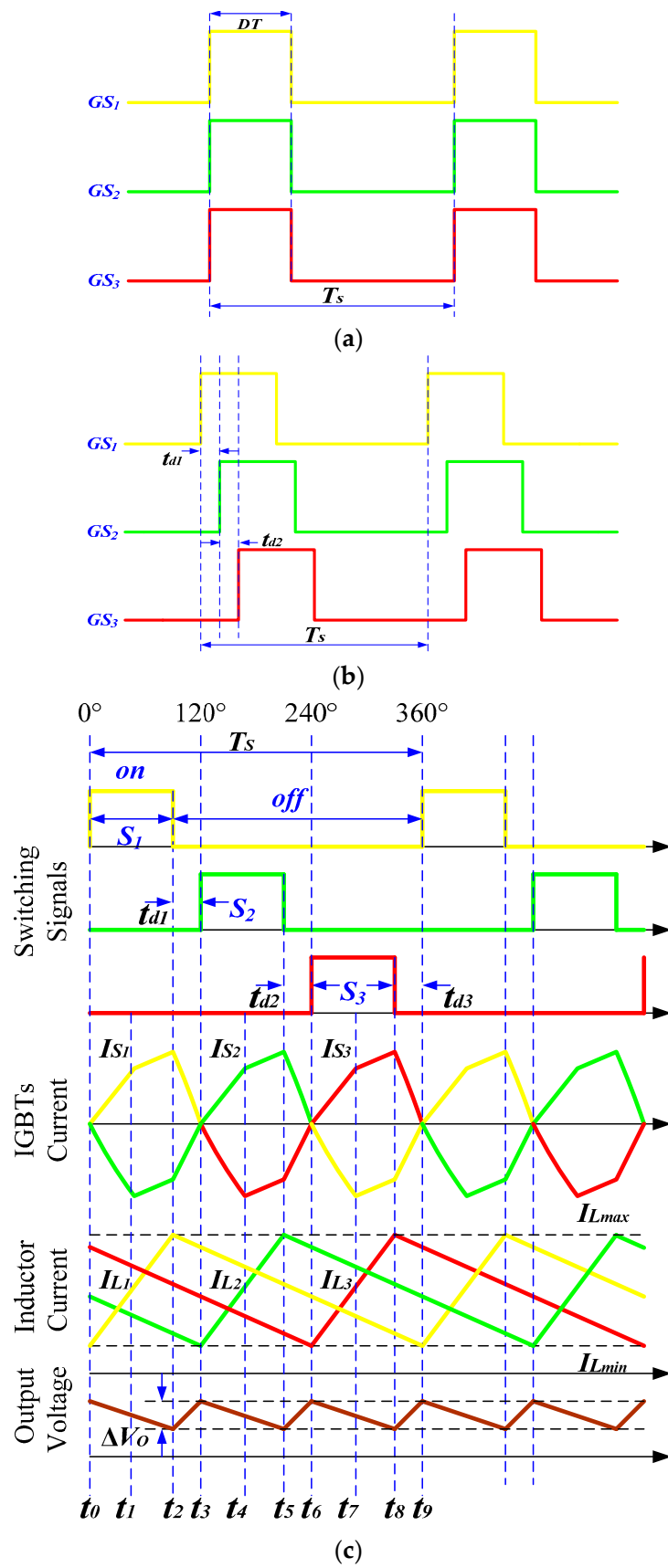


Figure 3. Driving signal key waveforms: (a) synchronized clocking, (b) phase-shift clocking, and (c) interleaving clocking.

2.2. Steady-State Analysis of the Studied Converter

The integrated converter circuit has three operation intervals: in the first interval, all switches are turned on; in the second interval, the active switch Q_1 is turned off while at least one of the other active switches is on; and in the third interval, all active switches are turned off. Figure 3c shows the steady-state voltage and current waveforms of the converter during one switching cycle covering the three operating intervals.

Under operation mode 1, $t \in [t_0-t_2, t_3-t_5, t_6-t_8]$, during which all of the switches are on and the inductors $L_1, L_2,$ and L_3 store the extracted energy from the energy sources, whereas the energy stored in the batteries in the preceding switching cycle is supplied to the grid through diodes $Dq_1, Dq_2,$ and Dq_3 .

Under operation mode 2, $t \in [t_0-t_1, t_3-t_4, t_6-t_7]$, during which S_1 is turned off and at least one switch S_n ($n = 2, 3, \dots,$ or m) is turned on. There are $2^{m-1} - 1$ different cases in this mode subject to the situations of the other $(m - 2)$ switching devices $S_2, \dots, S_{n-1}, S_{n+1}, \dots, S_m$. One case is explained as an example, in which only one switch S_n is turned on and all other switching devices are turned off.

Under operation mode 3, $t \in [t_2-t_3, t_5-t_6, t_8-t_9]$, during which all switches are off.

3. Control Strategy

The proposed converter has four ports, three of which are inputs consisting of PV panels, fuel cells, wind turbines, and a two-way battery storage port, as shown in Figure 4. The system uses three main switches through which zero-voltage switching is achieved. A unidirectional multiport boost DC-DC converter links the PV, FC, and WT with the DC-link, maintaining the stability of the converter system even with fluctuations in the load [26–28]. The energy can flow in only one direction from the PV, FC, and WT to the DC link. Using an appropriately designed MPPT algorithm, the PV, FC, and WT can be regulated to deliver maximum obtainable power from sunlight or wind using the studied converter. In the battery case, a bidirectional DC-DC converter is connected to the DC link and used as a battery charge regulator. The SOC battery charge is maintained around its reference value to obtain a high charging efficiency.

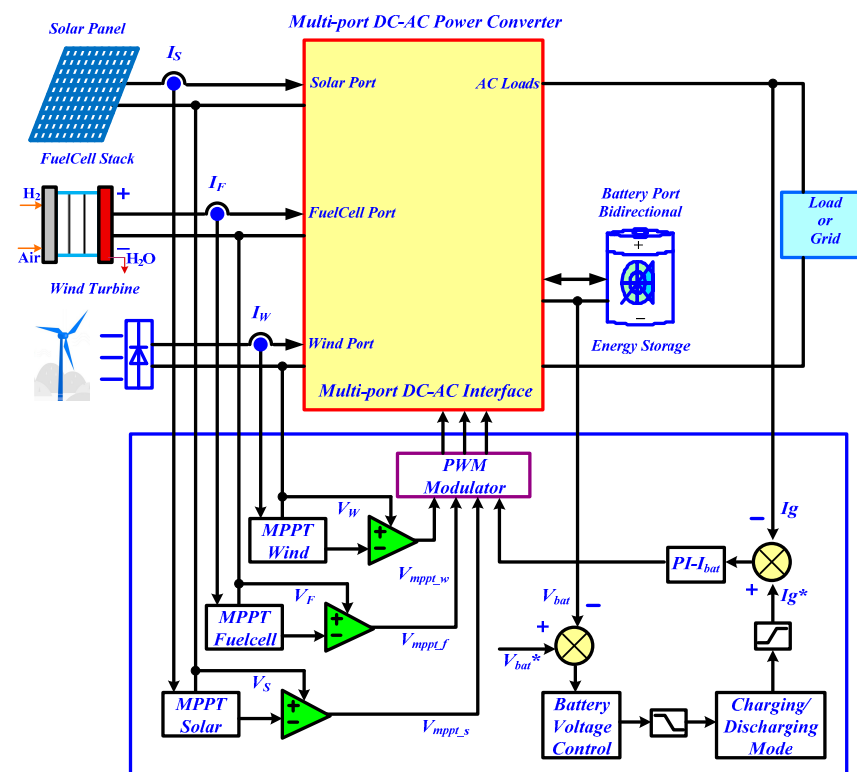


Figure 4. Control diagram of the studied multi-port DC-AC power converter.

This converter applies multiple functions: it acts as a regulator for charging the battery in a grid-connected operation and as a boost converter to deliver energy from the batteries to the microgrid when there is insufficient power from the solar cell sources, fuel cells, and wind turbines to feed the local loads during an island operation. Figure 5 shows a simplified bidirectional control structure. In order to reduce the switching loss and conduct a loss of IGBTs, the one-leg shoot-through procedure was chosen in the modulation strategy. The control strategy of the system is presented, as displayed in Figure 5, to deal with versatile load fluctuations.

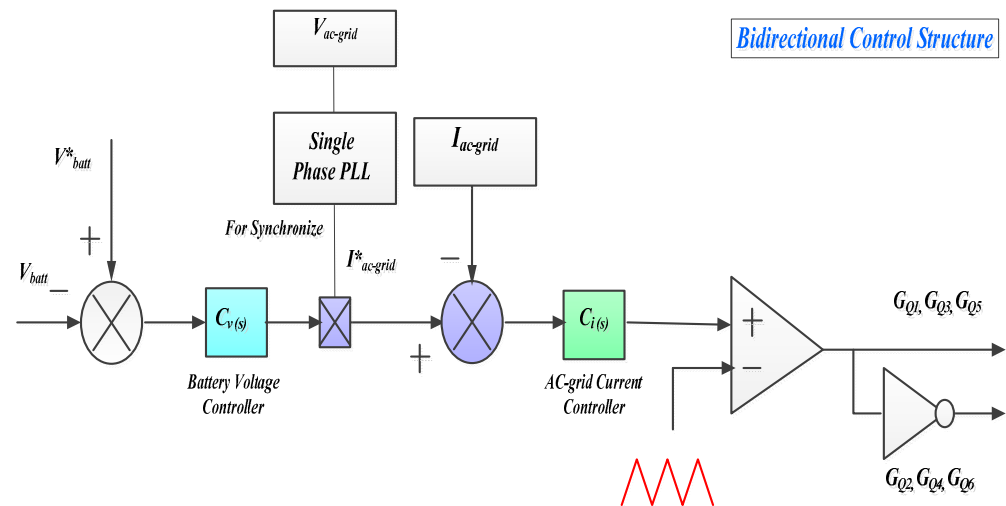


Figure 5. Structure of a dual-loop controller for the DC-AC inverter.

In Figure 5, the output voltage is regulated using the $C_v(s)$ regulator and is limited to a safe value generating the amplitude of input reference current. However, this reference signal is then multiplied with the output of the phase-locked-loop to synchronize the reference with the AC grid voltage. The inductor currents are required to follow its reference current using a current regulator $C_i(s)$, which produces suitable gateway signals. The major advantage of this controller is that it has a constant switching frequency.

3.1. PV Control Design for a Multiport DC-DC Converter

The MPPT methods differ according to the DC-DC converter topology and the related circuit parameters [29–31]. The panel voltage V_{pv} is sensed along with the PV input current I_{pv} before the input capacitance C_s . The MPPT algorithm uses these two values to track the MPP under different temperatures and irradiance levels. The reference point of the panel input is calculated and maintained at the MPP value, as shown in Figure 6. The MPPT is attained using a voltage loop (outer loop) and a current loop (inner loop), as shown in Figure 4. By increasing the current reference of the multiport converter, the output voltage decreases. Therefore, the signs of the voltage reference compensator and feedback are reversed. To avoid the output voltage from increasing higher than the component rating, the voltage feedback is planned for the internal comparators, which can make a cycle-by-cycle trip of the PWM during an overvoltage state. The I-V and P-V curves at different cell temperatures and a constant irradiation level can be obtained by measuring the PV voltage, current, and output power, as shown in Figure 6.

The values of open-circuit voltage V_{oc} and current of short-circuit I_{sc} related to the studied PV array are given in terms of the number of series and parallel cells:

$$V_{oc} = N_s * V_{oc,r} \quad (1)$$

$$I_{sc} = N_p * I_{sc,r} \quad (2)$$

The current versus voltage (I-V) characteristics of the PV panel can be expressed as follows [26,27]:

$$I_{ph} = S_n * I_{sc} + I_t(T_c - T_r), \quad (3)$$

Equation (3) can be used for a particular level of insolation S_n and at a specific operating temperature T_c of the PV cell.

$$I_d = I_o \left[\exp\left(\frac{q(V_L + I_L R_s)}{A k T}\right) - 1 \right], \quad (4)$$

$$I_o = I_{or} \left[\frac{T_c}{T_r} \right] \cdot \exp\left(\frac{q E_g}{B k} \left(\frac{1}{T_r} - \frac{1}{T_c} \right)\right), \quad (5)$$

$$I_L = I_{ph} - I_d - \left(\frac{V_L + I_L R_s}{R_{sh}} \right) \quad (6)$$

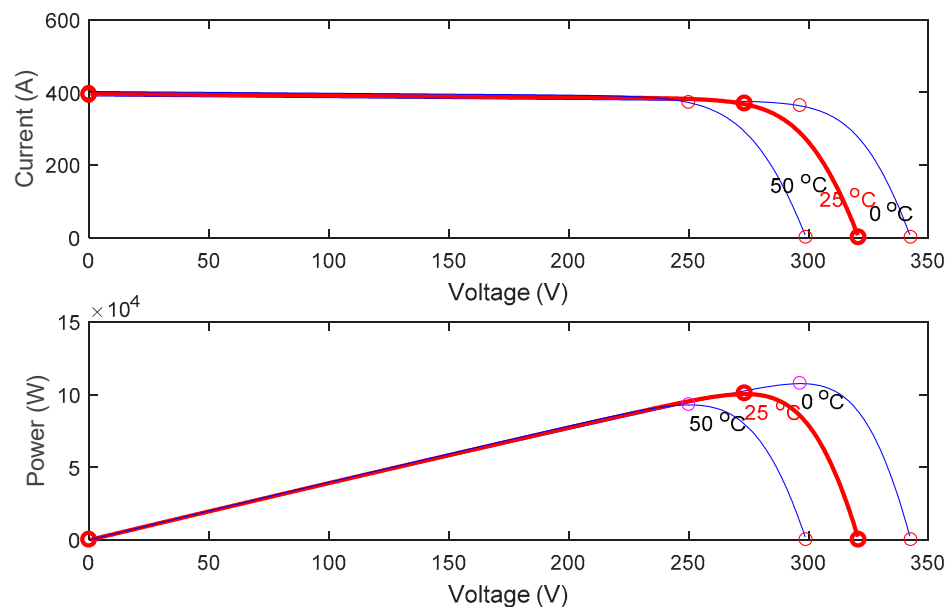


Figure 6. The I-V and P-V characteristic curves at different cell temperatures and a constant irradiation level.

3.2. FC Control Design for a Multiport DC-DC Converter

The control of the proposed converter comprises output-voltage stabilizing and current-limiting functions. A typical control is shown in Figure 4. The current limit is set at a stable level; however, for diverse sources, it can be adapted (e.g., for fuel cells, it should be proportionate to the H_2 fuel-injection, owing to the fuel cell characteristics), as shown in Figure 7. The current limit of the boost converter was adjusted to 30 A during the simulation tests. The DC voltage reference is also set to the fixed value required by the energy source integrated inverter with a microgrid or load. The energy excess or shortage can be determined from the reference value deviation. However, a power management system uses the deviation as an indicator of such situations. The voltage reference in this control strategy is the maximum value. When the DC voltage is higher than the reference value, this causes a decrease in the inductor current. When the battery SOC is lower than the reference value, the fuel cell supplies nearly the total power to the load. The implementation of this method is simple in comparison with the preceding schemes. Therefore, the PI controller gains are tuned online to improve the response.

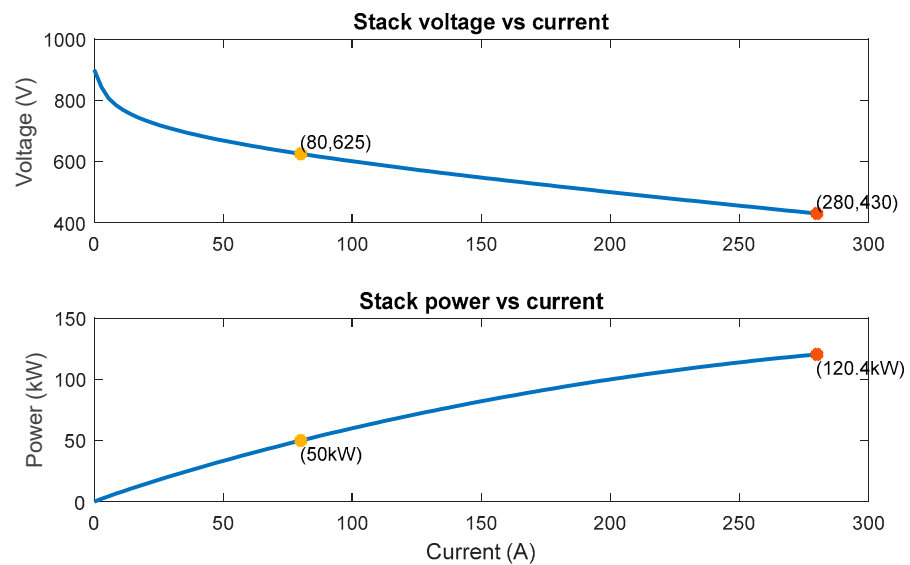


Figure 7. Stack voltage-current and power-current fuel cell characteristics.

3.3. WT Control Design for Multiport DC-DC Converter

The MPPs of the wind generator were estimated using the measured wind speeds. However, the other parameters are given by the manufacturer as follows:

$$P_{MPP(t)} = \begin{cases} \frac{1}{2} \cdot \rho \cdot \pi \cdot C_p \cdot r^2 \cdot v_{wind}^3 & v_{cut_in} < v_{wind} < v_{norm} \\ P_{norm} & v_{norm} \leq v_{wind} < v_{cut_out} \\ 0 & v_{wind} \leq v_{cut_in}, v_{wind} \geq v_{cut_out} \end{cases} \quad (7)$$

where P_{MPP} is the maximum power extracted from the wind turbine; v_{wind} is the wind speed, which can be measured using an anemometer; r is the radius of the wind turbine rotor plane; ρ is the air density; v_{cut_in} , v_{norm} , and v_{cut_out} are the cut-in, rated, and cut-out wind speeds of the wind turbine, respectively; P_{norm} is the rated power of the wind turbine, the value of which is equal to 60 kW; and C_p is the wind turbine power coefficient. According to Betz's law, the maximum value of the power coefficient C_p is 0.59. Conferring to the wind turbine characteristics (power-wind speed curves) given by the manufacturer, when the average wind speed is about 13.4 m/h, the monthly produced energy of the selected wind turbine is 60 kWh. Consequently, the maximum value of C_p was estimated to be 0.4457 for this wind turbine.

3.4. Battery Control Design

In this study, the power management in a microgrid is improved by the inclusion of backup energy storage, which consists of a set of batteries connected to a DC link through a bidirectional power converter. The bidirectional converter is composed of a boost inductor with inductance L , two switches (S_1 and S_2) allowing the bidirectional current flow, and an output filtering capacitor C_{dc} , as shown in Figure 8. With the power management method, there are two blocks used for controlling the voltage with suitable limitation blocks to achieve the required energy flow under different conditions. These controllers produce the current reference for the energy storage unit. The first controller adjusts the DC-link voltage and the second control block regulates the battery charge.

It is not advisable to discharge the energy storage battery deeply. However, at a low voltage level of the energy storage, there is a limited range of charging energies. This causes an over-voltage in the DC link during an energy recovery from the load side. For electrochemical batteries, the battery life has a limited range of discharge cycles, and the battery must be protected.

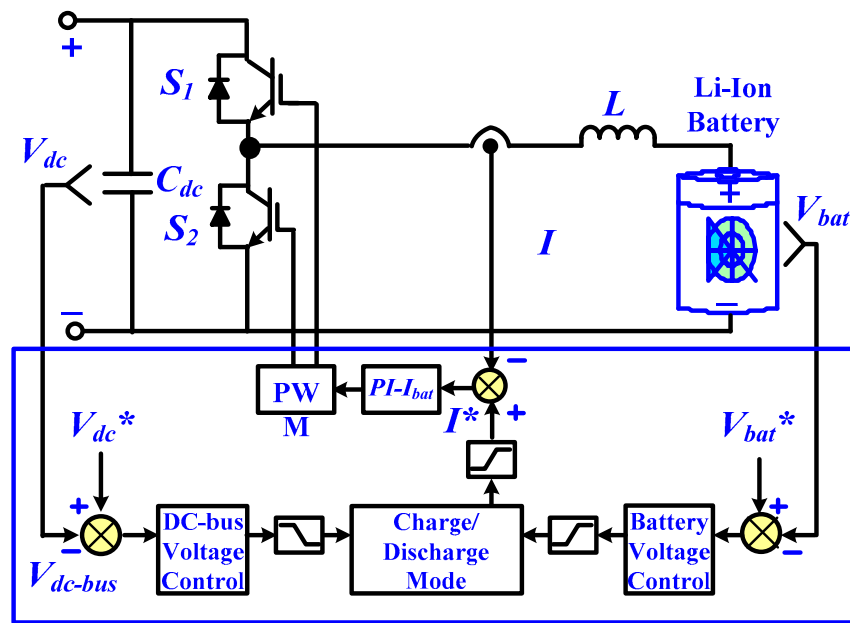


Figure 8. Bidirectional DC-DC converter battery port. Reproduced from [32], MDPI, 2019.

4. Simulation Results

Detailed simulation models were developed in a Simulink/MATLAB environment to verify the multi-port DC-DC power converter. These models present an alternative emergency power source established by fuel cells and lithium-ion batteries. An energy management system is included in the simulation model, which is suitable for many renewable energy sources. Simulation results were obtained according to the usual daily load profile of a commercial building in Majmaah city, as shown in Figure 9. The parameters of the proposed system are listed in Table 2. The parameters and technical specifications of the simulated PV Panels, PEM Fuel Cell, and wind turbine are listed in Appendix A (Tables A1–A3 respectively). The Simulink model of the proposed multiport DC-DC power converter is displayed in Figure 10.

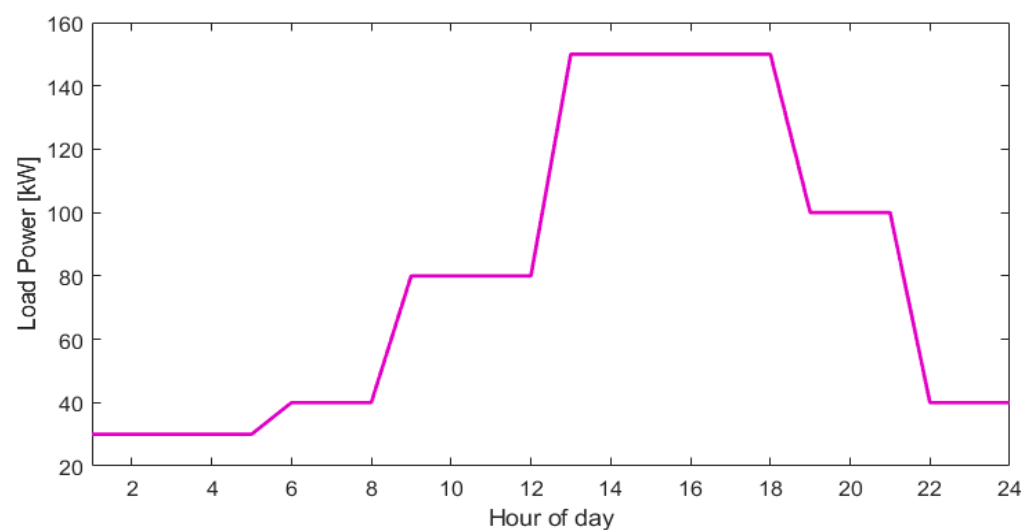


Figure 9. Selected building electricity load profile for the month of March.

Table 2. Parameters of studied system.

Item	Description
PV Panels	PV array comprising 330 modules (305 W) Series and parallel arrangement ($N_{ser} = 5, N_{par} = 66$) rated at 100 kW.
PEM (Proton Exchange Membrane) Fuel Cell	A 75 kW (peak), 625 V with power rating of 65 kW.
Wind Turbine	A 60 kWh at a wind speed about 2.5 m/s, the voltage amounts to 660 V.
Li-ion Battery	A 48 V, 400 Ah.
Inverter System	Rated 120 kVA, input 270 VDC, output 200 VAC, 60 Hz.

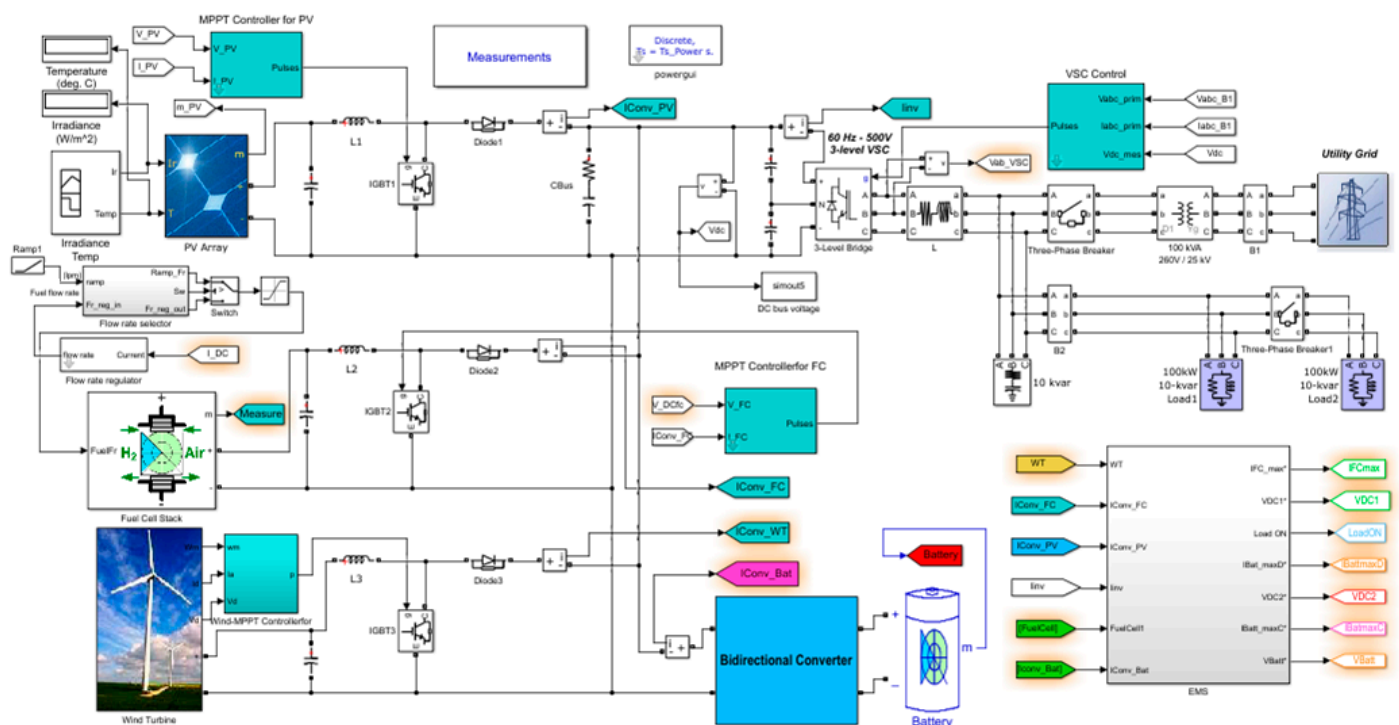


Figure 10. Simulink model of the proposed multi-port DC-AC power converter.

The MPPT control is utilized in the proposed converter to control the power produced by the PV panels, fuel cells, and wind turbine hybrid generation system, as shown in Figure 10. The controller is based on the P&O MPPT control technique [32–35] to make the best use of the power delivered from PV panels, fuel cells, and wind turbines simultaneously under different weather conditions. However, the wind speed changes more severely than the solar insolation and temperature. The output voltage and current of each renewable source are used by the MPPT controller as an input to produce a proper pulse-width modulated control signal for the corresponding active switch, as shown in Figure 10. A flowchart of the P&O MPPT algorithm is shown in Figure 11, where $P_s(k)$ is the power of each source at the k th step. For example, weather data such as solar insolation and ambient temperature are provided for calculating the quantity of energy that can be produced by solar PV panels. The PV output power value (P_{pv}) is compared with the power consumed by the load (P_L) to determine the energy flow distribution between the energy storage system and the load. The extra photovoltaic energy is stored in the energy storage unit (batteries) by a bidirectional DC-DC converter (P_{batt}). A flowchart of the control scheme for the PV/FC/WT hybrid generation system is shown in Figure 11. The control scheme can be divided into three cases as follows:

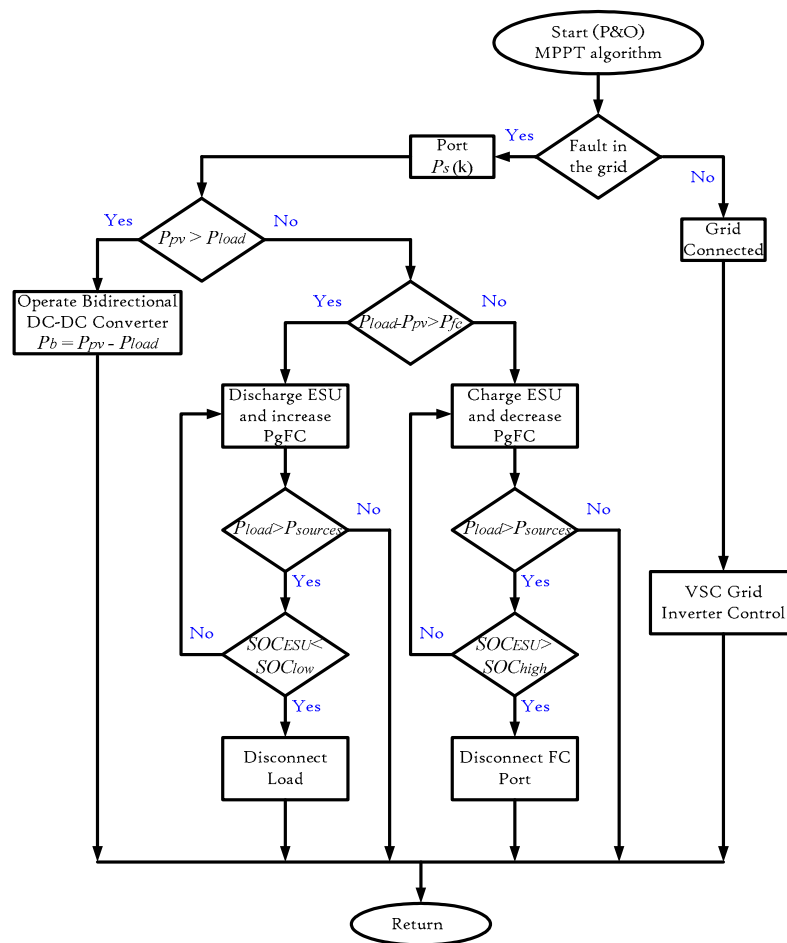


Figure 11. Flowchart of the P&O MPPT algorithm for the PV/FC/WT/ESU.

Case 1: $P_{pv} > P_L$, and thus $P_b = P_{pv} - P_L$. If the solar insolation value is satisfactorily high, the solar PV array supplies the load, and the surplus power is stored in the ESU (batteries) by the bidirectional DC-DC power converter.

Case 2: $P_{pv} < P_L$ and $P_L - P_{pv} \leq P_{fc}$, and thus, $P_L - P_{pv} = P_{fc}$. That is, if the PV source cannot supply the load, then the load is powered directly from the solar PV panel and the fuel cell is turned on.

Case 3: $P_{pv} < P_L$ and $P_L - P_{pv} > P_{fc}$, and thus, $P_L = P_{fc} = 0$ and $P_{wt} = P_{pv}$. In this case, the solar PV panel cannot empower the load, the fuel cell is turned off, and the load is supplied directly from the wind turbine generator, according to the conditions in Case 1 or 2.

Simulations were simulated for 25 s to validate the transient system behavior using a proportional-integral (PI) controller. Figure 12 shows the PV voltage and current. The PV power plant generation is regulated at the MPPT, which is proportional to the irradiance. The weather data were solar radiation (W/m^2), ambient temperature ($^{\circ}C$), and wind speed (m/h). Typical weather data were collected during 1-h intervals. There are numerous meteorological software packages that can calculate the solar insolation level, ambient temperature, and wind speed. The microgrid power generation reference is set to one real power step (at 25 s, Figure 12), and the sensed power of the microgrid is sufficiently close to the power reference. The battery recompenses the power deviations of the microgrid reference power, PV power, and total connected loads.

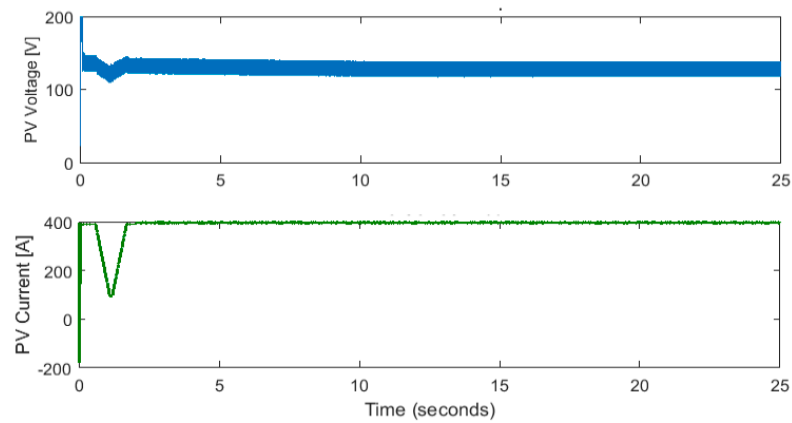


Figure 12. PV voltage and current.

Owing to the slow response time of the fuel cell, it can be observed that the fast power fluctuations can be reduced significantly using the energy storage unit, as shown in Figure 13. The FC will try to charge the ESU and increase the SOC if the load is not too high. Figure 14 shows the voltage and current waveforms of the fuel cell. Figure 15 shows the power delivered by the WT generator and the current waveforms. The battery voltage and current waveforms are presented in Figure 16. It should be noted that a positive current of ESU means that the ESU supplies the load and a negative current means that the ESU is charged. The AC load voltage and current waveforms are shown in Figure 17. The load current increased at 8 s and decreased at 20 s.

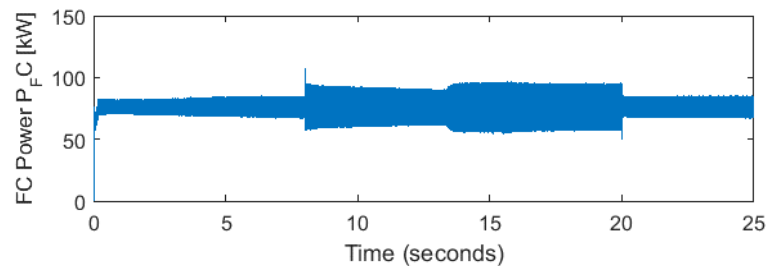


Figure 13. Fuel cell power.

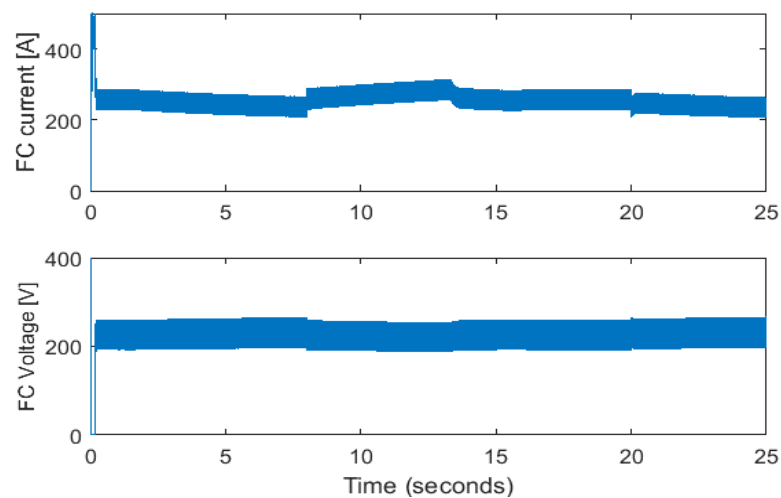


Figure 14. FC voltage and current.

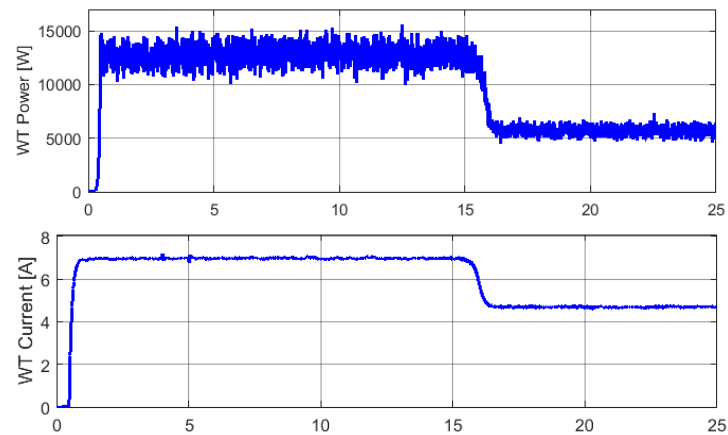


Figure 15. WT power and current waveforms.

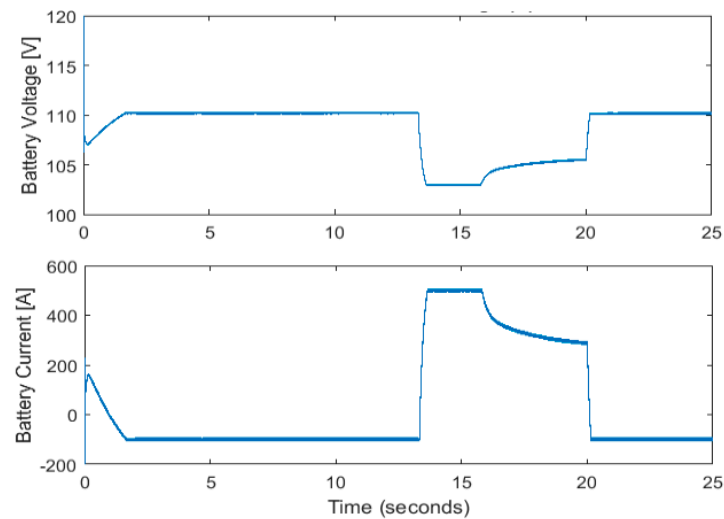


Figure 16. Battery voltage and current waveforms.

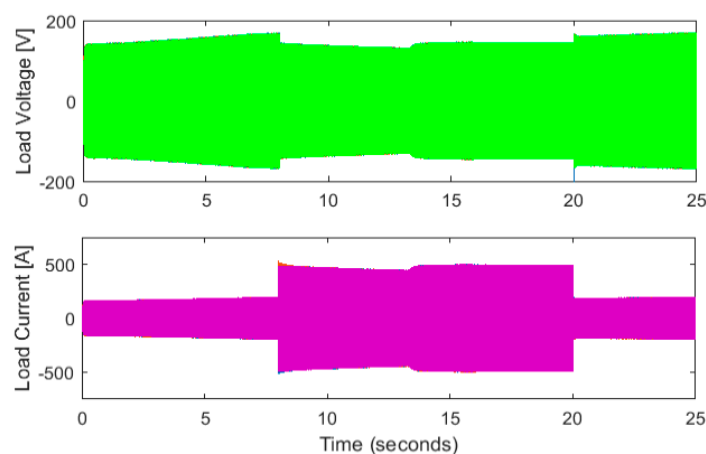


Figure 17. Load voltage and current.

Figures 18–20 show the simulation results. The output of the three-phase AC voltage and three-phase load current can be seen in Figure 17. The three-phase currents delivered by the AC inverter are sinusoidal owing to the use of AC filters, as shown in Figures 18 and 19. The converter can boost the DC link voltage from a 200 VDC input to a 400 V output voltage. The output current was approximately 7 A. However, the DC-link voltage and current waveforms are shown in Figures 20 and 21, respectively.

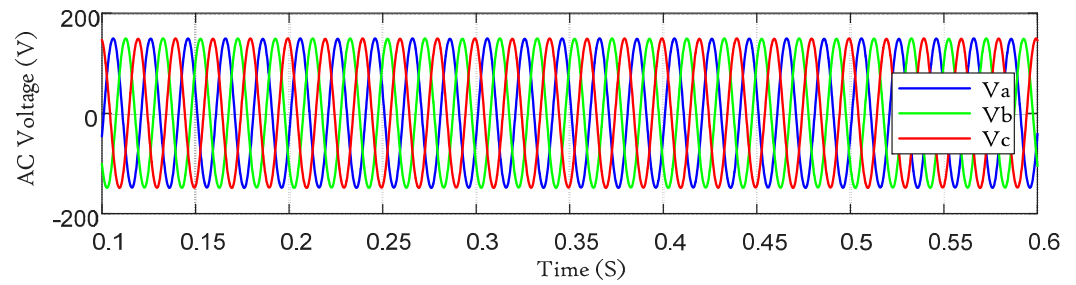


Figure 18. Three-phase AC inverter output voltage.

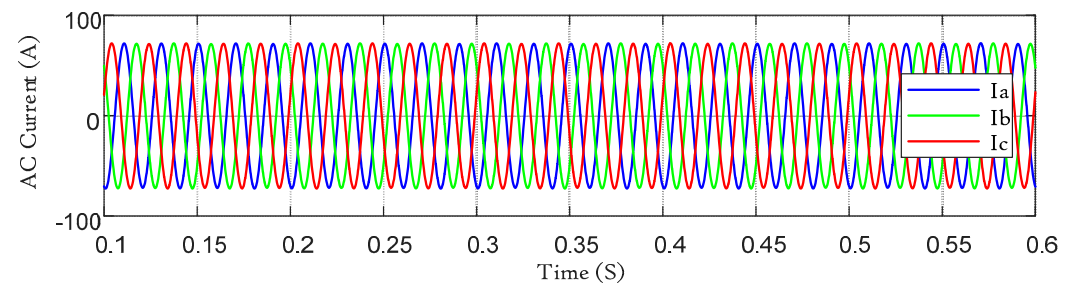


Figure 19. Three-phase AC inverter output current.

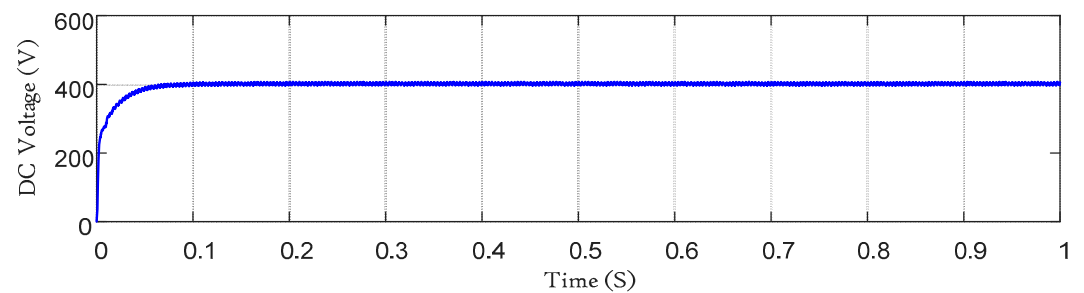


Figure 20. DC-link output voltage.

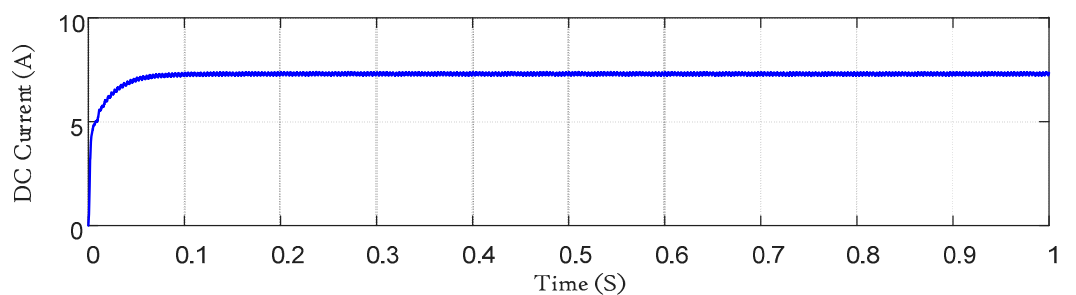


Figure 21. DC-link output current.

5. Experimental Verifications

The studied converter has been implemented in the hardware and power management of actual PV panels, fuel cells, and wind turbine hybrid generation systems. The proposed converter control was designed and implemented using a dSPACE controller. Figure 22 shows the experimental setup circuit consisting of a dSPACE 1202, AC load, 3 phase inverter, lithium-ion battery bank, voltage, and current sensors. The performance of the proposed converter was tested using a 300 W experimental prototype. The effectiveness of the proposed converter topology was demonstrated for renewable energy sources. The technical specifications and circuit parameters of the experimental converter prototype are listed in Table 3. The switching frequency of the DC-DC converter was selected as 10 kHz.

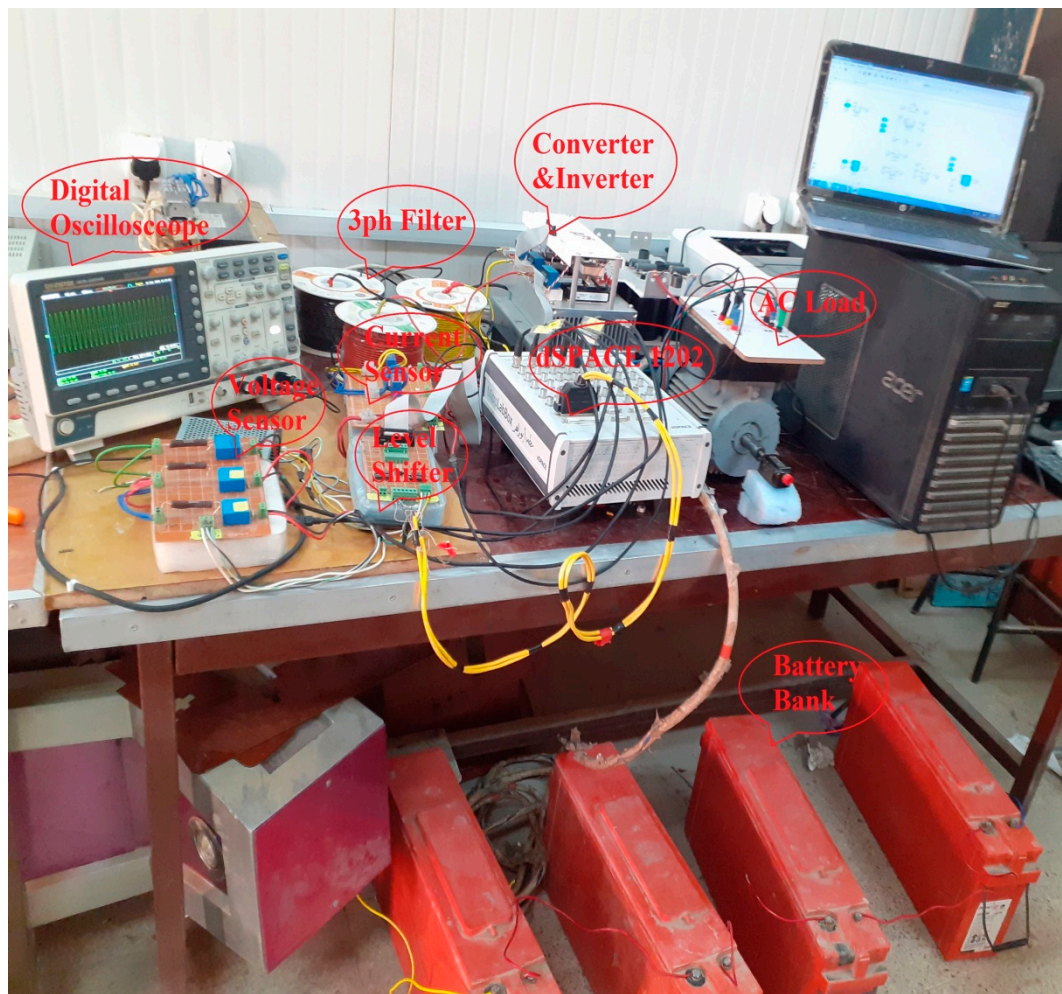


Figure 22. Experimental setup.

Table 3. Experimental specifications and parameters of the prototype multi-port DC-DC power converter.

Item	Symbol	Value	Item	Symbol	Value
DC-Input	V_{dc_in}	20 V	DC-Load Resistor	R_{L_dc}	50 and 100 Ω
DC-Output	V_{dc_out}	80 V	AC Load impedance	R_{L_ac} X_{L_ac}	78.97 Ω (balanced) 80 Ω
AC-Output	V_{ac_out}	20 V (peak)	DC-Capacitor	C_{dc}	330 μF
AC-Filter Inductance	L_{acf}	1200 μH	AC-Filter Capacitance	C_{acf}	10 μF

Figure 23 shows the gate-pulse sequence of the active switches of the proposed converter. The three gate pulses are sequenced for an interleaved clocking control scheme. Figure 24 displays the voltage waveforms across the active switches (S_1 , S_2 , and S_3). The voltage scale is 10 V per division. In addition, the peak switch voltage is approximately 25 V. Low-voltage stresses through the main active switches can be observed, which equal only one-third of the output voltage. The current waveforms through active switches are shown in Figure 25 (i_{ds1} , i_{ds2} , and i_{ds3}). In this figure, each voltage division is 1 A. However, the peak current through active switches is approximately 4 A.

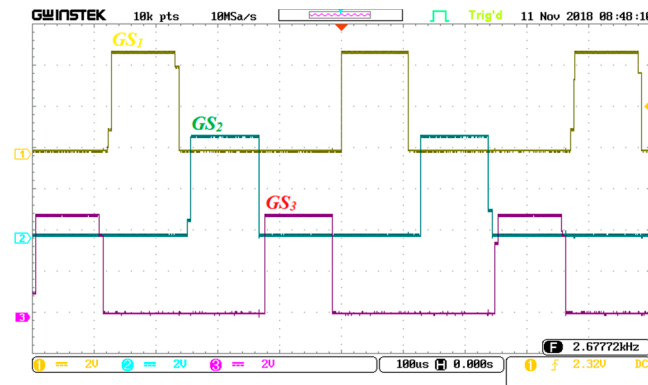


Figure 23. Gate-pulse sequence with interleaved clocking.

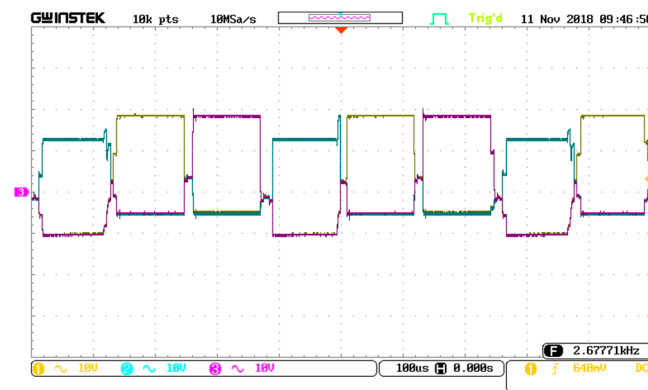


Figure 24. Voltage through switches V_{ds1} , V_{ds2} , and V_{ds3} .

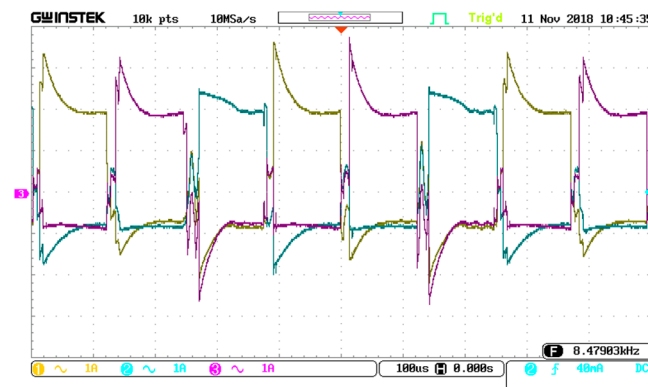


Figure 25. Currents through switches i_{ds1} , i_{ds2} , and i_{ds3} .

Figure 26 shows the waveforms for inductor currents (i_{L1} , i_{L2} , and i_{L3}). The balance between three currents through the boost inductors are shown. In this figure, the peak current in each inductor is approximately 4 A. The three-phase AC output voltages V_a , V_b , and V_c are shown in Figure 27. The input and output DC voltage waveforms are shown in Figure 28. In this figure, the voltage division is 5 V for the input voltage. Therefore, the input voltage is approximately 20 V. For the output of the voltage signal, the voltage division is 20 V. Consequently, the output voltage is approximately 80 V. In this case, the voltage gain is approximately 4-fold. Thus, the effectiveness of the proposed converter can be proved.

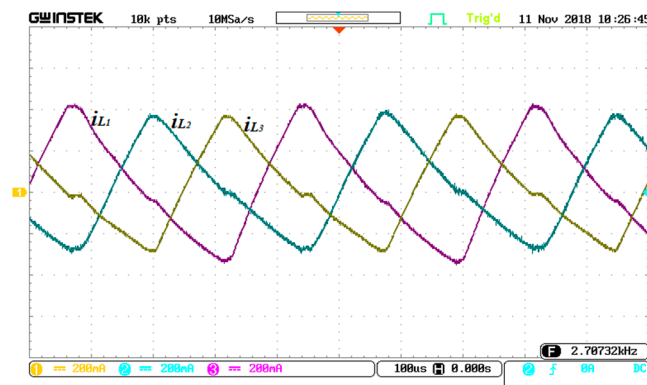


Figure 26. Currents through coupled inductors i_{L1} , i_{L2} , and i_{L3} .



Figure 27. Three-phase AC output voltages.

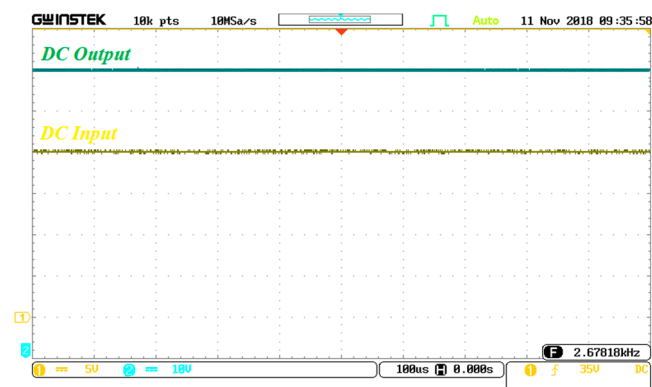


Figure 28. Input and output DC voltages waveforms.

6. Conclusions

In this paper, a multi-port DC-DC power converter was proposed for a synchronized power management of three renewable energy sources (PV panels, fuel cells, and wind turbines) and an energy storage source (batteries or supercapacitors). An energy management system, as well as control of DC-DC power converters, was developed. The simulation results indicate that the proposed energy management method achieves efficient power utilization. The battery energy storage compensates for the slow response of the fuel cells and photovoltaic units. The proposed strategy can share power between DG units, even under a different renewable power generation. An experimental prototype was applied to verify the effectiveness of the proposed multi-port converter topology. The advantages of the studied multiport PWM DC-DC power converter are the simplicity, reliability, and proficiency of MPPT control for several renewable energy sources at the same time. This

converter applies multiple functions: it acts as a regulator for charging the battery in a grid-connected operation and as a boost power converter to provide energy from the batteries to the microgrid when there is insufficient power from the solar cell sources, fuel cells, and wind turbines to feed the local loads during an island operation. Furthermore, the integrated converter can be efficiently utilized for the energy management of various renewable energy sources, including energy storage systems. In order to implement a prototype, we have used the real load profile to preserve the load pattern while we scaled down the load magnitude to be 3 KW.

Author Contributions: The author contributions are as follows; Conceptualization, K.S. and A.G.A.-K.; methodology, H.S.; software, A.A.; validation, A.A. and N.A.; formal analysis, A.A.; investigation, N.A.; resources, A.A.; data curation, A.G.A.-K.; writing—original draft preparation, K.S.; writing—review and editing, K.S.; visualization, H.S.; supervision, A.G.A.-K.; project administration, A.A.; funding acquisition, N.A. All authors have read and agreed to the published version of the manuscript.

Funding: This research received funding from the Deputyship for Research and Innovation, Ministry of Education in Saudi Arabia through project number (IFP-2020-03).

Institutional Review Board Statement: Not applicable.

Informed Consent Statement: Not applicable.

Data Availability Statement: The data that support the findings of this study are available on request from the corresponding author.

Acknowledgments: The authors extend their appreciation to the Deputyship for Research and Innovation, Ministry of Education in Saudi Arabia, for funding this research work through project number (IFP-2020-03).

Conflicts of Interest: The authors declare no conflict of interest.

Appendix A

Table A1. Datasheet of the PV Panels.

DC Electrical Characteristics	Specifications
STC Power Rating	305 W
PTC Power Rating	282.1 W ¹
STC Power per unit area	187.0 W/m ² (17.4 W/ft ²)
Peak Efficiency	18.7%
Power Tolerances	−5%/+5%
Number of Cells	96
Imp	5.58 A
Vmp	54.7 V
Isc	5.96 A
Voc	64.2 V
NOCT	45 °C
Isc Temperature. Coefficient	0.06%/K
Temp. Coefficient of Power	−0.38%/K
Temp. Coefficient of Voltage	−0.173V/K
Series Fuse Rating	15 A
Maximum System Voltage	600 V
Mechanical Characteristics	

Table A1. *Cont.*

DC Electrical Characteristics	Specifications
Type	Monocrystalline Silicon
Output Terminal Type	Multicontact Connector Type 4
Output Cable Wire Gauge	12 AWG
Output Cable Wire Type	PV Wire
Output Cable Wire Length	1000 mm (39.4 in)

Table A2. Datasheet of the PEM (Proton Exchange Membrane) Fuel Cell.

Datasheet	PEMFC
Number of Cells	24
Rated Power	65 kW
Peak Power	75 kW
Operating Temp.	50–80 °C
Power Density	350 mW/cm ²
Fuel Efficiency	45–60 Chem. to Elec.
Reactants	Hydrogen and Air
Lifetime	>40,000 h
Area of Application	Portable, Mobile, Stationary

Table A3. Datasheet of the Wind Turbine.

Power	Specification
Power rating	60 kW
Cut-in wind speed	2.5 m/s
Wind speed rating	9.0 m/s
Cut-out wind speed	25 m/s
Survival wind speed	50 m/s
Rotor	
Diameter	21 m
Swept area	346.4 m ²
Number of blades	3
Max. Rotor speed	50 U/min
Tipspeed	55 m/s
Type	10 m
Material	Fiberglass reinforced composite. Resin Transfer Molding (RTM)
Power density 1:	173.2 W/m ²
Power density 2:	5.8 kW/m ²
Generator	
Type	Permanent magnet alternator
Number	1
Maximum Speed	50 U/min
Voltage	660 V
Grid frequency	50/60 Hz

References

1. Das, D.; Esmaili, R.; Xu, L.; Nichols, D. An Optimal Design of a Grid Connected Hybrid Wind/Photovoltaic/Fuel Cell System for Distributed Energy Production. In Proceedings of the 31st Annual Conference of IEEE Industrial Electronics Society, IECON 2005, Raleigh, NC, USA, 6–10 November 2005; p. 6.
2. El-Khattam, W.; Hegazy, Y.; Salama, M. Stochastic Power Flow Analysis of Electrical Distributed Generation Systems. In Proceedings of the 2003 IEEE Power Engineering Society General Meeting, Toronto, ON, Canada, 13–17 July 2003; pp. 141–143. [\[CrossRef\]](#)
3. El-Khattam, W.; Hegazy, Y.; Salama, M. Stochastic Estimation of the Contribution Levels of Customer Operated Distributed Generation. In Proceedings of the IEEE Power Engineering Society General Meeting, Denver, CO, USA, 6–10 June 2004; pp. 2182–2186.
4. Solero, L.; Caricchi, F.; Crescimbeni, F.; Honorati, O.; Mezzetti, F. Performance of a 10 kW Power Electronic Interface for Combined Wind/PV Isolated Generating Systems. In Proceedings of the PESC Record—27th Annual IEEE Power Electronics Specialists Conference, Baveno, Italy, 23–27 June 1996; pp. 1027–1032.
5. Chen, Y.-M.; Liu, Y.-C.; Wu, F.-Y.; Wu, T.-F. Multi-Input DC/DC Converter Based on the Flux Additivity. In Proceedings of the Conference Record of the 2001 IEEE Industry Applications Conference—36th IAS Annual Meeting, Chicago, IL, USA, 30 September–4 October 2001; pp. 1866–1873. [\[CrossRef\]](#)
6. Kassakian, J.G.; Jahns, T.M. Evolving and Emerging Applications of Power Electronics in Systems. *IEEE J. Emerg. Sel. Top. Power Electron.* **2013**, *1*, 47–58. [\[CrossRef\]](#)
7. Lucia, O.; Cvetkovic, I.; Sarnago, H.; Boroyevich, D.; Mattavelli, P.; Lee, F.C. Design of Home Appliances for a DC-Based Nanogrid System: An Induction Range Study Case. *IEEE J. Emerg. Sel. Top. Power Electron.* **2013**, *1*, 315–326. [\[CrossRef\]](#)
8. Carr, J.; Balda, J.C.; Mantooth, A. A High Frequency Link Multiport Converter Utility Interface for Renewable Energy Resources with Integrated Energy Storage. In Proceedings of the 2010 IEEE Energy Conversion Congress and Exposition, Atlanta, GA, USA, 12–16 September 2010; pp. 3541–3548. [\[CrossRef\]](#)
9. Qiao, W.; Sharma, A.; Hudgins, J.L.; Jones, E.G.; Rilett, L.R. Wind/Solar Hybrid Generation-Based Roadway Microgrids. In Proceedings of the 2008 IEEE Power and Energy Society General Meeting—Conversion and Delivery of Electrical Energy in the 21st Century, Detroit, MI, USA, 24–28 July 2011; pp. 1–7.
10. Qian, Z.; Abdel-Rahman, O.; Batarseh, I. An Integrated Four-Port DC/DC Converter for Renewable Energy Applications. *IEEE Trans. Power Electron.* **2010**, *25*, 1877–1887. [\[CrossRef\]](#)
11. Shen, C.-L.; Yang, S.-H. Multi-Input Converter with MPPT Feature for Wind-PV Power Generation System. *Int. J. Photoenergy* **2013**, *2013*, 1–13. [\[CrossRef\]](#)
12. Li, Q.; Wolfs, P. A Review of the Single Phase Photovoltaic Module Integrated Converter Topologies with Three Different DC Link Configurations. *IEEE Trans. Power Electron.* **2008**, *23*, 1320–1333. [\[CrossRef\]](#)
13. Wang, Z.; Li, H. Integrated MPPT and Bidirectional Battery Charger for PV Application Using One Multiphase Interleaved Three-Port Dc-Dc Converter. In Proceedings of the 2011 Twenty-Sixth Annual IEEE Applied Power Electronics Conference and Exposition (APEC), Fort Worth, TX, USA, 6–11 March 2011; pp. 295–300.
14. Wang, Z.; Li, H. An Integrated Three-Port Bidirectional DC–DC Converter for PV Application on a DC Distribution System. *IEEE Trans. Power Electron.* **2013**, *28*, 4612–4624. [\[CrossRef\]](#)
15. Forest, F.; Meynard, T.A.; Labouré, E.; Gelis, B.; Huselstein, J.-J.; Brandelero, J.C. An Isolated Multicell Intercell Transformer Converter for Applications with a High Step-Up Ratio. *IEEE Trans. Power Electron.* **2012**, *28*, 1107–1119. [\[CrossRef\]](#)
16. Su, G.-J.; Peng, F. A low cost, triple-voltage bus DC-DC converter for automotive applications. In Proceedings of the Twentieth Annual IEEE Applied Power Electronics Conference and Exposition, APEC 2005, Austin, TX, USA, 6–10 March 2005; pp. 1015–1021. [\[CrossRef\]](#)
17. Chen, Y.-M.; Huang, A.Q.; Yu, X. A High Step-Up Three-Port DC–DC Converter for Stand-Alone PV/Battery Power Systems. *IEEE Trans. Power Electron.* **2013**, *28*, 5049–5062. [\[CrossRef\]](#)
18. Blaabjerg, F.; Ma, K. Future on Power Electronics for Wind Turbine Systems. *IEEE J. Emerg. Sel. Top. Power Electron.* **2013**, *1*, 139–152. [\[CrossRef\]](#)
19. Wu, H.; Chen, R.; Zhang, J.; Xing, Y.; Hu, H.; Ge, H. A Family of Three-Port Half-Bridge Converters for a Stand-Alone Renewable Power System. *IEEE Trans. Power Electron.* **2011**, *26*, 2697–2706. [\[CrossRef\]](#)
20. Li, W.; Xiao, J.; Zhao, Y.; He, X. PWM Plus Phase Angle Shift (PPAS) Control Scheme for Combined Multiport DC/DC Converters. *IEEE Trans. Power Electron.* **2012**, *27*, 1479–1489. [\[CrossRef\]](#)
21. Sayed, K.; El-Zohri, E.H.; Mahfouz, H. Analysis and design for interleaved ZCS buck DC-DC converter with low switching losses. *Int. J. Power Electron.* **2017**, *8*, 210–231. [\[CrossRef\]](#)
22. Shum, K.; Ashley, C. A New Full Shunt Switching Unit for Solar Array Using Coupled-Inductor Boost Converter. In Proceedings of the IECEC 96—31st Intersociety Energy Conversion Engineering Conference, Washington, DC, USA, 11–16 August 1996; pp. 617–622.
23. Veerachary, M.; Senjyu, T.; Uezato, K. Maximum power point tracking of coupled inductor interleaved boost converter supplied PV system. *IEE Proc. Electr. Power Appl.* **2003**, *150*, 71. [\[CrossRef\]](#)
24. Zumel, P.; Garcia, O.; Cobos, J.; Uceda, J. Magnetic Integration for Interleaved Converters. In Proceedings of the Eighteenth Annual IEEE Applied Power Electronics Conference and Exposition, 2003, APEC '03, Miami Beach, FL, USA, 9–13 February 2003; pp. 9–13.

25. Dahono, P.; Riyadi, S.; Mudawari, A.; Haroen, Y. Output Ripple Analysis of Multiphase DC-DC Converters. In Proceedings of the IEEE 1999 International Conference on Power Electronics and Drive Systems, PEDS '99, Hong Kong, China, 27–29 July 1999; pp. 27–29.
26. Sayed, K.; Abdel-Salam, M.; Ahmed, A.; Ahmed, M. New High Voltage Gain Dual-boost DC-DC Converter for Photovoltaic Power Systems. *Electr. Power Compon. Syst.* **2012**, *40*, 711–728. [[CrossRef](#)]
27. Kwon, S.K.; Sayed, K.F. Boost-half bridge single power stage PWM DC-DC converters for PEM-fuel cell stacks. *J. Power Electron.* **2008**, *8*, 239–247.
28. Sayed, K.; Abdel-Salam, M. Dynamic performance of wind turbine conversion system using PMSG-based wind simulator. *Electr. Eng.* **2017**, *99*, 431–439. [[CrossRef](#)]
29. Anowar, M.H.; Roy, P. A modified Incremental Conductance Based Photovoltaic MPPT Charge Controller. In Proceedings of the 2019 International Conference on Electrical, Computer and Communication Engineering (ECCE), Cox's Bazar, Bangladesh, 7–9 February 2019; pp. 1–5.
30. Sera, D.; Mathe, L.; Kerekes, T.; Spataru, S.V.; Teodorescu, R. On the Perturb-and-Observe and Incremental Conductance MPPT Methods for PV Systems. *IEEE J. Photovolt.* **2013**, *3*, 1070–1078. [[CrossRef](#)]
31. Figueiredo, S.N.; Aquino, R.; Zurita, M.E.P.V. Comparison Between PO-Based and PSO-Based MPPT Algorithms for Photovoltaic System Under Partially Shaded Conditions. In Proceedings of the 6th International Conference on Control, Decision and Information Technologies (CoDIT), Paris, France, 23–26 April 2019; pp. 685–690.
32. Sayed, K.; Abo-Khalil, A.G.; Alghamdi, A.S. Optimum Resilient Operation and Control DC Microgrid Based Electric Vehicles Charging Station Powered by Renewable Energy Sources. *Energies* **2019**, *12*, 4240. [[CrossRef](#)]
33. Sayed, K.; Ali, Z.M.; AlDhaifallah, M. Phase-Shift PWM-Controlled DC–DC Converter with Secondary-Side Current Doubler Rectifier for On-Board Charger Application. *Energies* **2020**, *13*, 2298. [[CrossRef](#)]
34. Sayed, K.; Gronfula, M.G.; Ziedan, H.A. Novel Soft-Switching Integrated Boost DC-DC Converter for PV Power System. *Energies* **2020**, *13*, 749. [[CrossRef](#)]
35. Hua, C.; Lin, J.; Shen, C.; Hua, C.; Lin, J.; Shen, C. Implementation of a DSP-controlled photovoltaic system with peak power tracking. *IEEE Trans. Ind. Electron.* **1998**, *45*, 99–107. [[CrossRef](#)]